Characterization of a clinical unit for digital radiography based on irradiation side sampling technology

Stefano Rivetti
Fisica Medica, Ospedale di Sassuolo S.p.A., 41049 Sassuolo, Italy

Nico Lanconelli[a)]
Alma Mater Studiorum, Physics Department, University of Bologna, 40127 Bologna, Italy

Marco Bertolini and Andrea Nitrosi
Medical Physics Unit, Azienda Ospedaliera ASMN, Istituto di Ricovero e Cura a Carattere Scientifico, 42123 Reggio Emilia, Italy

Aldo Burani
Ospedale di Sassuolo S.p.A., 41049 Sassuolo, Italy

(Received 8 March 2013; revised 1 August 2013; accepted for publication 15 August 2013; published 10 September 2013)

Purpose: A characterization of a clinical unit for digital radiography (FUJIFILM FDR D-EVO) is presented. This system is based on the irradiation side sampling (ISS) technology and can be equipped with two different scintillators: one traditional gadolinium-oxysulphide phosphor (GOS) and a needle structured cesium iodide (CsI) phosphor panel.
Methods: The characterization was achieved in terms of response curve, modulation transfer function (MTF), noise power spectra (NPS), detective quantum efficiency (DQE), and psychophysical parameters (contrast-detail analysis with an automatic reading of CDRAD images). For both scintillation screens the authors accomplished the measurements with four standard beam conditions: RAQ3, RQA5, RQA7, and RQA9.
Results: At the Nyquist frequency (3.33 lp/mm) the MTF is about 35% and 25% for CsI and GOS detectors, respectively. The CsI scintillator has better noise properties than the GOS screen in almost all the conditions. This is particularly true for low-energy beams, where the noise for the GOS system can go up to a factor 2 greater than that found for CsI. The DQE of the CsI detector reaches a peak of 60%, 60%, 58%, and 50% for the RQA3, RQA5, RQA7, and RQA9 beams, respectively, whereas for the GOS screen the maximum DQE is 40%, 44%, 44%, and 35%. The contrast-detail analysis confirms that in the majority of cases the CsI scintillator is able to provide improved outcomes to those obtained with the GOS screen.
Conclusions: The limited diffusion of light produced by the ISS reading makes possible the achievement of very good spatial resolution. In fact, the MTF of the unit with the CsI panel is only slightly lower to that achieved with direct conversion detectors. The combination of very good spatial resolution, together with the good noise properties reached with the CsI screen, allows achieving DQE on average about 1.5 times greater than that obtained with GOS. In fact, the DQE of unit equipped with CsI is comparable to the best alternative methods available which are based on the same technology, and similar to others based on an a-Se direct conversion detectors. © *2013 American Association of Physicists in Medicine*. [http://dx.doi.org/10.1118/1.4820364]

Key words: digital radiology, irradiation side sampling, modulation transfer function, detective quantum efficiency

1. INTRODUCTION

The traditional field of projection x-ray imaging went through a significant transformation into the digital age during the last decade. Digital radiography (DR) has become an everyday technique in clinical practice since the beginning of this century. Its popularity around the world is mainly a result of the increased availability of flat panel detectors (FPDs) on the market. FPDs are constituted of two main components: an x-ray conversion layer (such as phosphor or photoconductor) that transforms the incident x-ray energy into a distribution of secondary quanta (such as light photons or electron-hole pairs) and a detector that measures this secondary quantum field. Two types of FPDs have been developed: direct and indirect systems. In the former x rays are directly converted into electron–hole pairs, whereas in the latter x rays are first converted into visible light photons that are then detected by photosensitive elements.[1–3] The majority of indirect FPDs available on the market employ an x-ray converter made of gadolinium oxysulfate (GOS), while some FPDs are available with cesium iodide (CsI) scintillators. It is important that the scintillation layer absorbs as many of the incident x-ray photons as possible. This can be achieved by increasing the thickness of the scintillator, although this must

be done while maintaining sufficient spatial resolution for the particular clinical task.

For a conventional indirect FPD system, the scintillator and the photodiode are arranged in the front and the back to the incident direction of x rays, respectively. This configuration causes considerable attenuation and diffusion of light in the scintillator, especially for thick scintillation layers. A variant on the design of indirect detectors consists of mounting the photodiode array on the anterior side of the detector, the so-called irradiation side sampling (ISS) technique. This orientation allows the light photons to exit the scintillator from the x-ray incidence surface. As a matter of fact, with the ISS system the layers of the flat panel detector are in reverse order to conventional detector.[4,5] The benefit of this configuration is a reduction of light attenuation and blurring effects. In fact, due to the energy deposition profile of the x rays into the depth of the phosphor material, the ISS design can significantly improve the spatial resolution of the system. It has already been shown that the use of an ISS system allows one to increase the thickness of the scintillator layer thus improving the sensitivity without reducing the spatial resolution. This gives rise to an improved detective quantum efficiency (DQE) of the system.[4,5]

One of the technologies available for improving the image quality of an indirect FPD system is to use columnar scintillators (e.g., CsI crystals). Indeed, CsI crystals can be grown in a dense, needle-like (5–10 μm in diameter) structure, in layers with thickness up to 600 μm. The generated fluorescent light can therefore be guided to the photodetector array without much lateral dispersion, as happens with optical fibers. The "light piping" properties for light generated within the needles allow these materials to be deposited in a significantly thicker layer than a traditional powdered phosphor while maintaining a similar spatial resolution. CsI-based FPD systems with thicker scintillation layers can increase the x-ray absorption, thus improving the noise properties, while the spatial resolution capabilities are maintained. In other words, the CsI scintillator, thanks to its needle structure, is able to deliver high image sharpness and to provide a spatial resolution better than the conventional GOS screens. In addition, the inherent morphology of the needle-like structure also allows the effective packing density of the layer to more closely approach the single crystal density, which further improves the x-ray absorption.

The aim of this paper is to characterize two clinical units for digital radiography based on an indirect conversion detector with ISS technology (named FUJIFILM FDR D-EVO), through physical figures of merit (MTF, NPS, and DQE), and psychophysical parameters (CD analysis).[6] The two units were equipped with two different scintillators: one with CsI phosphor (Model plus C35i) and one with GOS (Model G35i).

2. MATERIALS AND METHODS

For conventional indirect conversion flat panel detectors, x rays enter the phosphor layer and come out of the photodiode. On the other hand, for ISS detectors, the incident side for x rays is the glass substrate (Fig. 1). This may affect the outcome of the process. In fact, with traditional flat panels the DQE of the detector usually increases for small increases in the value of the phosphor thickness, whereas when the phosphor thickness is too large the DQE could reach a plateau or even decreases. In other words, in such systems there is a limit on how much one may increase the effective absorption via (the) thickening of the phosphor layer. In contrast, for ISS systems it is possible to increase the integral DQE even for very thick phosphor layers, as reported in Ref. 5. Besides, the ISS system can also be advantageous in terms of point spread function, especially for very thick phosphor layers. In fact, for conventional systems, the spread of the emitted light increases when the layer is increased. Figures 1(a) and 1(b) illustrate this property. Instead, as depicted in Figs. 1(c) and 1(d), for ISS systems the spread at the x-ray entrance does not change even if the phosphor layer is increased.

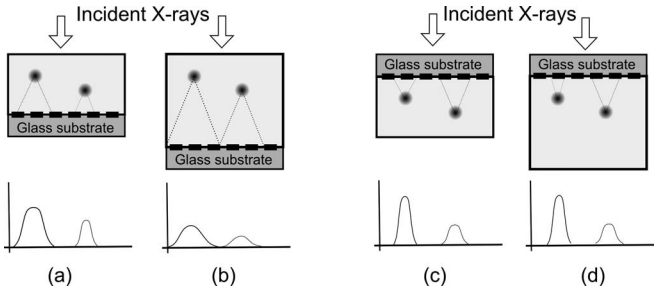

FIG. 1. Simplified representation of the attenuation and spreading of light for thin (a) and (c) and thick (b) and (d) phosphor layers in the conventional (a) and (b) and irradiation side (c) and (d) technologies. In the conventional technique, the intensity and spread of light degrades as the thickness of the phosphor increases. On the other hand, for the irradiation side method the response does not change when the phosphor thickness increases.

Two FDR D-EVO systems were considered, differing in the scintillator layer: the first one used a conventional GOS (Gd_2O_2S) screen (Model G35i) while the second one was based on a CsI structured scintillator (Model plus C35i). We tested both systems and in this paper we present their characterization and a comparison of their performance. The main characteristics of the investigated systems are reported in Table I. More details about the investigated systems can be found in the literature.[5]

All measurements were achieved for four different beam conditions: RQA3, RQA5, RQA7, RQA9, as defined by IEC standards.[7] For the added filtration, we used aluminum type 1199 (99.99% purity). The exposure to the detector was

TABLE I. Main characteristics of the investigated systems.

Manufacturer	FUJIFILM
System	FDR D-EVO
Detection type	Indirect conversion
Detector material	[GOS] − [CsI]
Imaging area (cm × cm)	35 × 43
Array size	2304 × 2880
Pixel pitch (μm)	150
Image depth (bits)	12

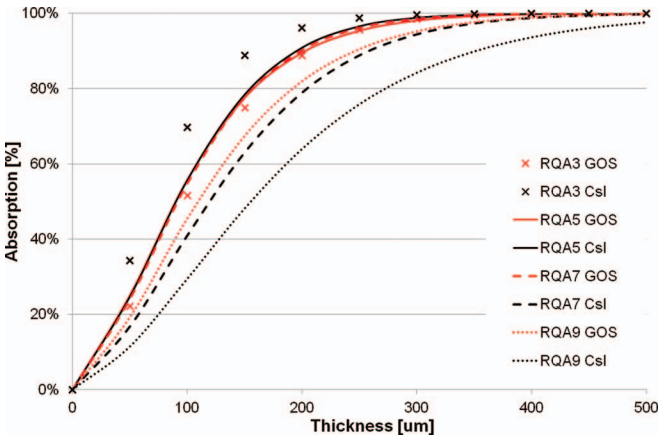

FIG. 2. Absorption curves for the two detectors as a function of the detector thickness for the four x-ray beams. To derive the curves, density values of 4.51 and 7.1 g/cm^3 and packing density of 100% and 75% have been considered for CsI and GOS, respectively.

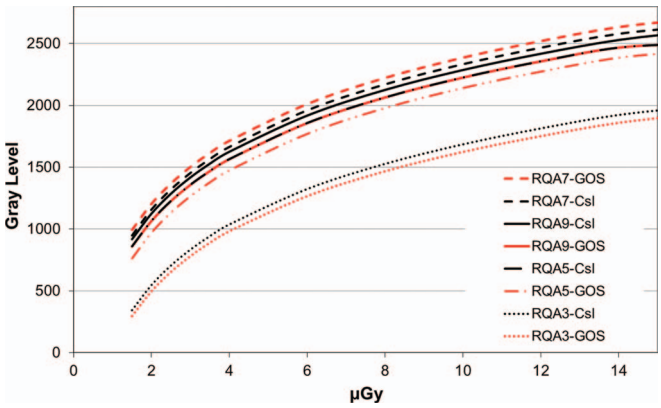

FIG. 3. Response curve for the two detectors at the four considered x-ray beams (RQA3, RQA5, RQA7, and RQA9). The response is logarithmic for all the x-ray conditions and fittings were achieved with a $R^2 > 0.99$.

measured using a calibrated ionization chamber (UNFORS Xi, Unfors Instruments, Billdal, Sweden). The source-to-detector distance was chosen to be around 180 cm for all the measurements.

In digital chest radiography the ratio of the maximum to minimum x-ray exposures incident on the detector surface can be greater than 100:1.[8] However, the most interesting range analyzed for characterizing detectors for digital radiography is from about 1 μGy to an upper limit of around 10 μGy, as reported and considered by many authors.[9–19] Hence, in this paper we achieved the characterization of the clinical unit in the range 1–15 μGy.

All systems manufactured by FUJIFILM, both for computed and direct radiography adopt the same image processing technology. The readout electronics generates 16 bit linear data, and a subsequent logarithmic transform is applied to the data, giving rise to a 12 bit image. The 16 bit linear image is never accessible to users, whereas the 12 bit data are made available through one of the processing modes. In fact, users are required to choose among one of the processing methods (automatic, semiautomatic, FIX mode, and others). The FIX mode is the only one that allows users to keep under control all the parameters, as the sensitivity (S) and latitude (L) values, such that the pixel values in the resultant image are directly linked to exposure in a manner that mimics a film screen system. All the images used in this work were acquired with the FIX mode processing using the following two sets of reading process parameters: $S = 200$ and $L = 3$, and the CRF filter set to "OFF."[18] The FIX-mode is typically chosen to get unprocessed images for achieving the physical characterization, when a FUJIFILM unit was included.[16,20–22] The system was calibrated with the standard clinical procedures. Since some sort of image processing is inherent to the images coming from these devices, and some details of the image processing are unknown, this could limit the validity and interpretation of the measurements reported. Nevertheless, comparison of the measurements between the two similar ISS systems is of practical interest, whereas the direct comparison of these measurements to those of other systems (acquired without image processing) should be carefully considered.

2.A. Response curve

The response curve was determined by exposing the detector to a wide range of values for uniform x-ray exposures. For each quality beam the response curves were fitted with a logarithmic function in the analyzed dose range.

The relative sensitivity S_i is estimated to be the ratio between the air kerma needed at a certain beam energy to the same signal obtained with a reference beam (in our case the RQA5 beam). In practice, we calculated S_i at a predetermined air kerma value (2 μGy) with the following formula:

$$S_i = \frac{\int E \cdot \phi_i(E) \cdot (1 - \exp(-\mu(E) \cdot t)) \cdot dE/D_i}{\int E \cdot \phi_{RQA5}(E) \cdot (1 - \exp(-\mu(E) \cdot t)) \cdot dE/D_{RQA5}} \quad (1)$$

where E is the energy, μ is the linear attenuation coefficient for the detector material, t is the detector thickness, D is the air kerma value, and ϕ is the photon fluence at the detector incident surface. The relative sensitivity calculated via Eq. (1) is then compared to the one calculated via experimental data.

2.B. Physical characterization

Due to the logarithmic response, all images used for the physical measurements were linearized by using the fitted response function. The quantitative comparison was achieved by calculating MTF, NPS, and DQE, as reported by IEC standards.[23]

Presampling MTF was measured by using the edge technique: an oversampled edge spread function was obtained by a tungsten edge test device (TX5, IBA Dosimetry, Schwarzenbruck, Germany). MTF was calculated along both directions, horizontal and vertical, and finally presented as the average along the two directions. NPS was computed by means of flood images acquired at various exposure levels. We calculated the 2D NPS from averaging the Fourier transformations

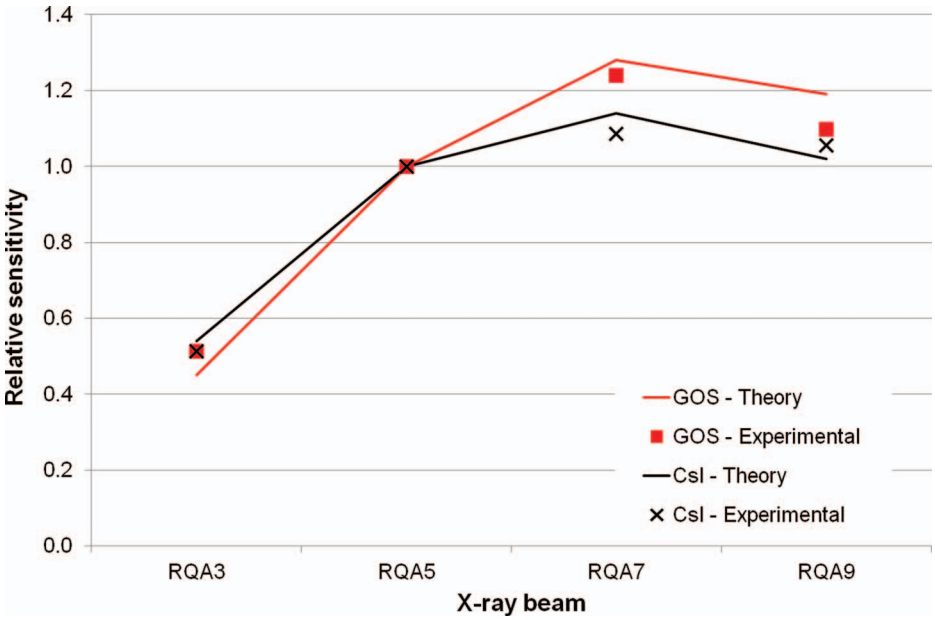

FIG. 4. Relative sensitivity for the two detectors at an exposure of about 2 μGy. Theoretical values are derived from Eq. (1).

of fixed-size ROIs (256 × 256 pixels) extracted from four different images at each exposure. The 1D NPS was then extracted from the 2D NPS along the horizontal and vertical directions, excluding the central axes, and averaged for the evaluation of the DQE. To assess the quantum-noise-limited conditions of the detector, the product of the NPS and exposure (air kerma) was also evaluated. The DQE was finally calculated as

$$\mathrm{DQE}(f) = \frac{\mathrm{MTF}^2(f)}{\mathrm{NPS}(f,q)\cdot q}, \tag{2}$$

where q is the number of photons per unit area. For each beam condition we used tabulated data for the photon fluence. MTF, NPS, and DQE were calculated by using an ImageJ plugin freely available at the site www.medphys.it.

2.C. Contrast-detail analysis

We realized a contrast-detail (CD) analysis of the two systems by means of an automatic reading of the CDRAD 2.0 phantom (Artinis, Medical Systems B.V., Zetten, The Netherlands). To this end, we acquired four images for each exposure level. The exposure values were the same as those used for the physical characterization. In order to avoid the remains of small details in the same detector area, the phantom was repositioned after each exposure. We used inhouse

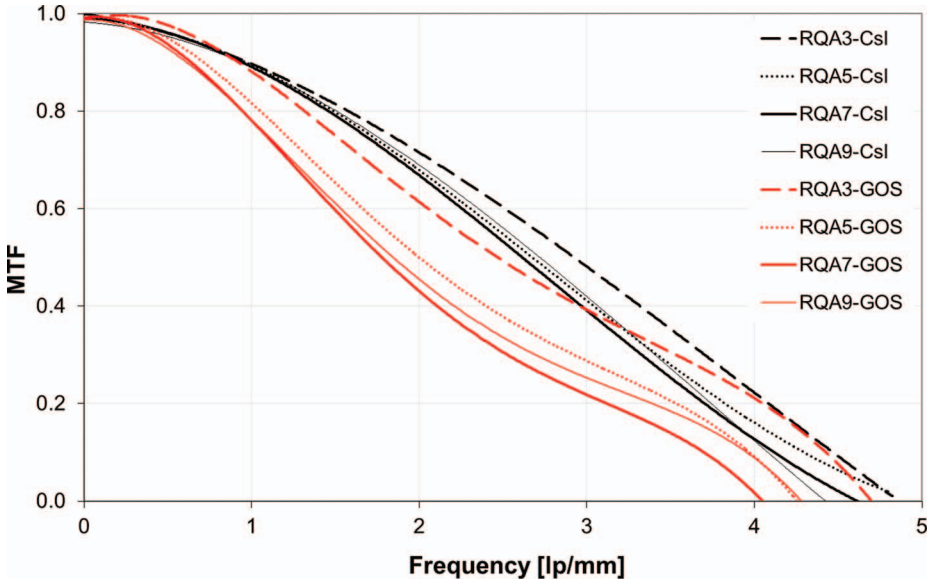

FIG. 5. Modulation transfer function of the two detectors for the four considered x-ray beams. The MTF for the CsI panel is remarkably better than the GOS one. There are no appreciable differences between the MTF along the horizontal and vertical direction. Here we show the MTF estimated from the average of the two directions.

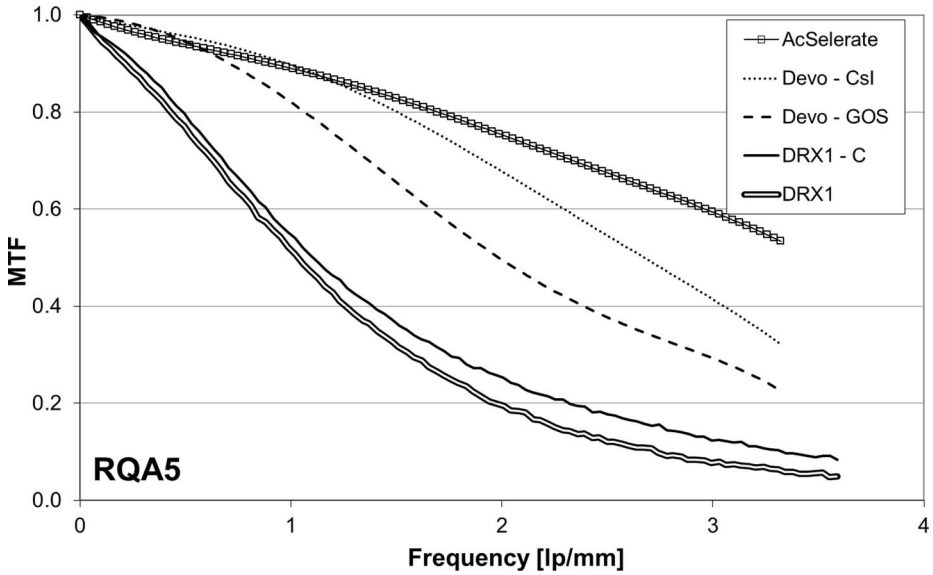

FIG. 6. Comparison of the MTF obtained for the two detectors (D-EVO–CsI and D-EVO–GOS) for the RQA5 beam with some of the best data available from the literature: system based on a thick a-Se layer (AcSelerate), other indirect-conversion systems based on GOS (DRX1) and CsI (DRX1-C) scintillators.

software written in IDL^{TM} (ITTVIS, Pearl East Circle Boulder, USA) to achieve the automatic reading of the images. This also may be freely downloaded from www.medphys.it. More details about the functioning of this software can be found in the literature.[18] From the CD analysis we derived the image quality figure (IQF) defined as follows:

$$\mathrm{IQF} = \sum_{i=1}^{15} D_i \cdot C_{i,th}, \tag{3}$$

where D_i is the diameter of the details in row i and $C_{i,th}$ denotes the threshold contrast in row i. Summation over all diameter rows yields the IQF; the smaller the IQF, the better the visibility of the details.

3. RESULTS AND DISCUSSION

Figure 2 shows the absorption curves for the two detectors as a function of their thickness for the four considered x-ray beams. Spectra for the four x-ray beams were calculated by using the software Spekcalc, developed by the Institute of Cancer Research in London (UK) and freely available on the web.[24] Density values of 4.51 and 7.1 g/cm^3 were used for CsI and GOS, respectively, for calculating the absorption values. A packing density value of 75% was considered for the GOS layer, according to data available from the literature,[5] whereas for CsI we utilized a packing density of 100%. The absorption curves can give some hints with regards to the depth of interaction of the x rays: indeed at least half of the fluence is stopped in less than 150 μm, even for the most energetic beams. We can thus observe that many of the light emissions happen in the proximity of the incident surface. As a consequence, the diffusion of light is limited with the ISS system, whereas it results larger for conventional systems, especially those with thick scintillators. We also note that for CsI the absorption efficiency continuously decreases with increasing x-ray energy. This is due to the position of the K-edge of cesium and iodine (36 and 33 keV, respectively). In contrast,

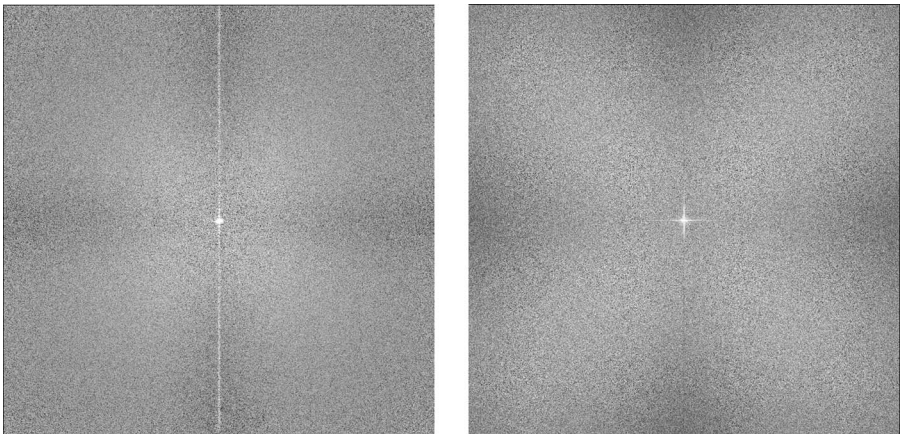

FIG. 7. 2D noise power spectrum for the two detectors at an exposure of around 2.5 μGy (RQA5 beam condition): GOS (left) and CsI (right). The contrast of the images has been adjusted for achieving a better visibility of the pictures.

due to its 50 keV K-edge, for GOS the absorption efficiency is almost constant across the different energies.

3.A. Response curve

In Fig. 3 the response curves for all the considered conditions (four x-ray beams and two scintillator materials) are reported. We fitted a logarithmic function to the experimental data; all fittings were achieved with (a) $R^2 > 0.99$ in the dose range between 1 and 15 μGy. For both scintillators the response of the system to the RQA3 beam is remarkably different to those achieved with all other beams. This is due to the different sensitivity of the detector material to the various energies of the incoming x rays, as shown in Fig. 4, both for experimental data and theoretical values derived from Eq. (1), using estimated thickness of 0.2 and 0.5 mm for GOS and CsI, respectively. The two systems present a peak response at the RQA7 beam, as also reported by other authors.[10] However, for RQA5, RQA7, and RQA9 beams the sensitivity is similar, and this is reflected also in the similar response curve shown in Fig. 3.

3.B. Physical characterization

Figure 5 shows the presampling MTF estimated with the edge technique, for the four different x-ray beams and the two detectors. MTF resulted to be independent from both the exposure values and the direction of the edge. Here we present MTFs calculated as the mean of the horizontal and vertical directions. At the Nyquist frequency (3.33 lp/mm) the MTF is about 35% and 25% for CsI and GOS detectors, respectively. It is worth noting that all the MTFs decrease to zero in a smooth and continuous way, thus indicating a negligible influence of image processing or noise in the line spread function.

These outcomes are better than most of the ones obtained from other systems available on the market,[10,11,17,19,25] as reported in Fig. 6. This is in accordance to the better properties in terms of spatial resolution claimed for ISS systems. Moreover, the CsI panel presents MTF for a wide range of frequencies comparable to that achieved with direct conversion detectors and about 20% worse at the Nyquist frequency, as shown in Fig. 6.[18] It is worth noting that when the CsI scintillator is considered there is clear improvement of the MTF, for all the x-ray beams. In fact, an average improvement of about 30% can be observed for the CsI FPD, in agreement to some of the data from the literature for systems dedicated to breast imaging.[26,27] This confirms that the reduction of light spread by the needle structure of the scintillator is effectively able to improve the spatial resolution of the system. All digital radiography systems are subject to large area glare resulting from internal x-ray scatter. This lateral signal spread can be expected to result in a relatively rapid decrease in MTF at low spatial frequencies. From our data it is hard to deduce different low-frequency drops for the two phosphors.

In Fig. 7 an example of 2D NPS is presented, for both detectors at an exposure of about 2.5 μGy. For both systems the NPS shape is more uniform than expected for a

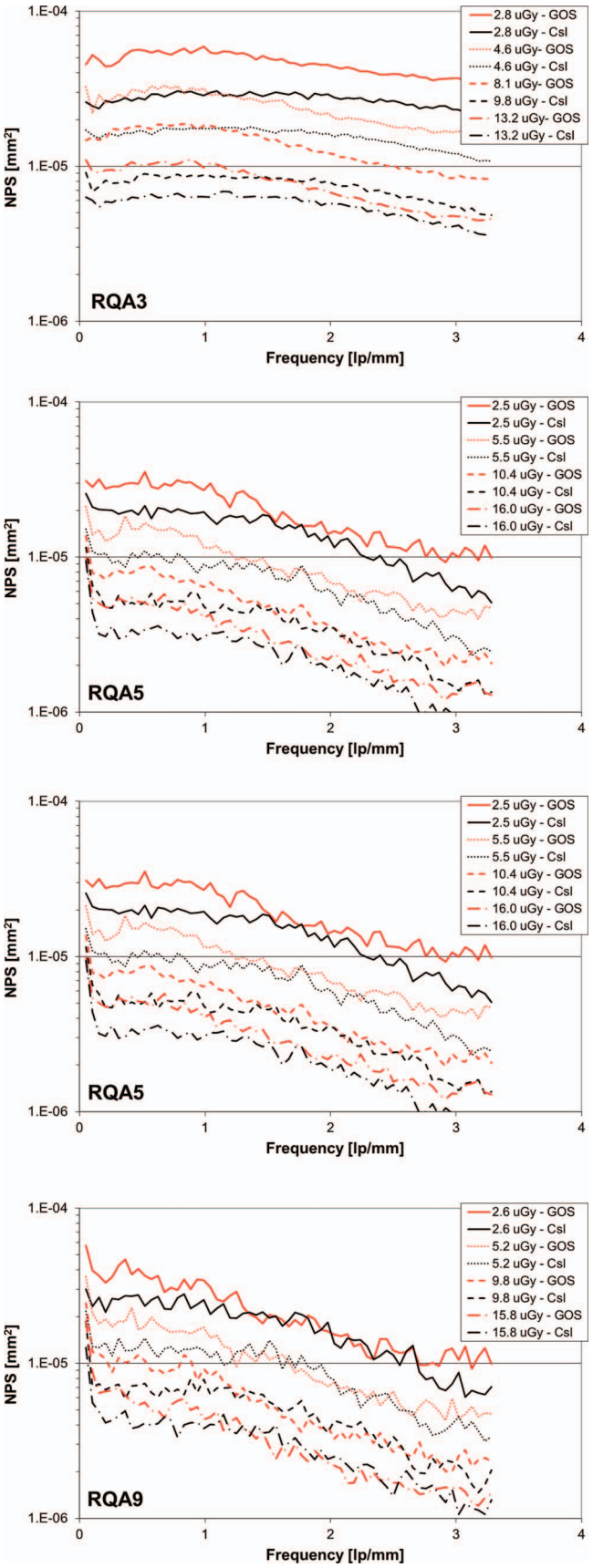

FIG. 8. NPS for the two detectors at various exposure values for the four investigated beams (RQA3, RQA5, RQA7, and RQA9). In the majority of conditions the CsI detector is able to provide noise properties better than the GOS one.

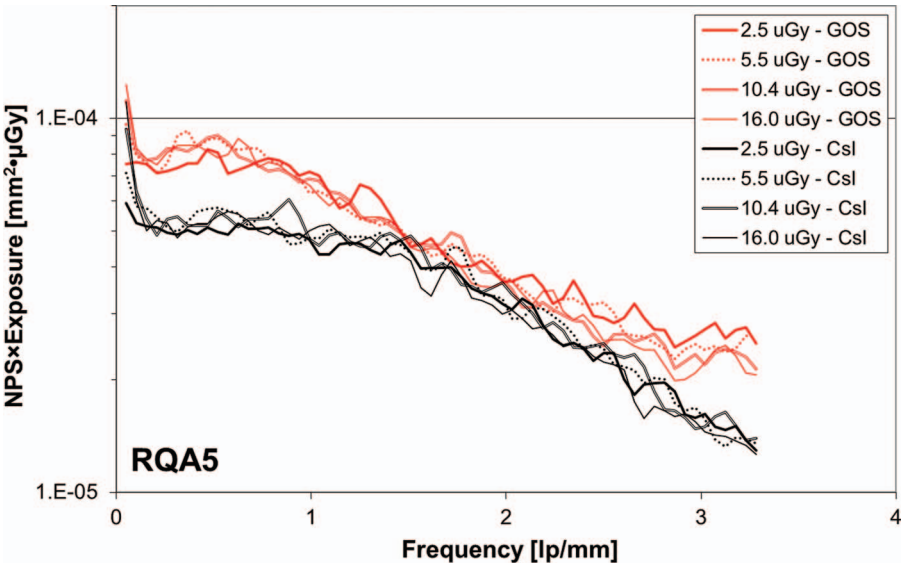

FIG. 9. NPS multiplied by air kerma for the RQA5 beam. For most cases this product is reasonably independent from the exposure, meaning that both detectors are in a quantum noise limited condition.

conventional indirect detector. In fact, the steep fall in NPS with spatial frequency, typical for the scintillator based FPDs, can hardly be observed here: this is due to the better MTF achievable with ISS reading, when compared to conventional systems, as reported in the literature.[5] Analyzing the 2D spectra it seems that some sort of processing is applied to the images; as already observed for other systems from FUJIFILM.[9,15–17,26,28–30] In fact, in this case a 1D sharpness filter seems to be applied by the acquisition software along the principal directions, causing a decreasing of the noise along the axes.

Figure 8 shows the NPS of the two systems at various exposure levels for the four investigated beams. We note that the CsI scintillator, thanks to the greater thickness of the scintillation layer, is able to improve the GOS screen noise properties in many conditions. This was expected and indeed had already been reported in the literature.[31] In particular, for the low-energy beams, the improvement of the CsI is clear and the noise for the GOS system can go up by a factor 2 greater than that found for CsI. On the contrary, at high energies the NPS of the GOS is shown to be comparable or even lower at high spatial frequencies.

Figure 9 shows the product of the NPS and the exposure for the two detectors for the RQA5 beam, whereas in Fig. 10 the same product is presented for all the beams at an exposure of 5 μGy. These values confirm that, in terms of noise spectra, the CsI detector is generally better than the one based on GOS. Further, from Fig. 9 we can affirm that both

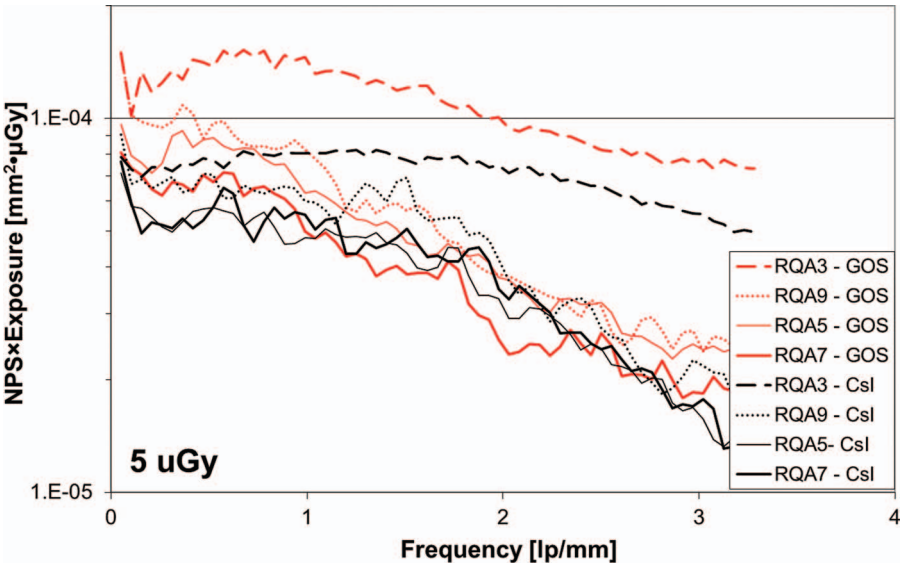

FIG. 10. NPS multiplied by air kerma at and exposure of around 5 μGy for the four investigated beams. As has already been noted, the CsI detector can provide better noise properties.

detectors are in quantum noise limited condition in the entire range of investigated exposure levels. The poor sensitivity for the RQA3 beam is responsible for the poor outcomes of this beam. This also can clearly be seen, for both scintillators, from Fig. 9.

In Fig. 11 the DQE of the two detectors at various exposure levels for the four beams is presented. Again, the CsI scintillator clearly improves the outcomes of the system in all the investigated conditions. The DQE of the CsI system is on average about 1.5 times that of the GOS one, even if the improvement is higher at low energies and lower at high energies. The DQE of the CsI detector reaches a peak of 60%, 60%, 58%, and 50% for the RQA3, RQA5, RQA7, and RQA9 beams, respectively. For GOS, the maximum DQE is 40%, 44%, 44%, and 35% for the RQA3, RQA5, RQA7, and RQA9, respectively. Across the various energies we can see a remarkable decrease of the performance for the CsI panel for the most energetic beam. On the contrary, the GOS response is not very dependent from the energy of the x-ray beam. From the DQE plots we also notice that the system is in the quantum noise limited condition in almost all the cases. This is since the DQE is not strongly dependent on the exposure.

Figure 12 shows the DQE of the two systems for the four beams at an exposure of 5 μGy. Both systems present a non-negligible dependence on the x-ray beam resulting from the different outcomes obtained at the various energies in terms on sensitivity, MTF and NPS. The DQE of the CsI panel continuously drops with increasing energy, whereas the GOS presents a peak for the RQA7 beam. This is a direct consequence of the absorption properties of the two materials, as shown in Fig. 2 and also reported by other authors.[29,32] It is well known that clinical units based on CsI screens might not be advantageous for chest radiography, where the high tube voltage used makes the use of GOS scintillators profitable. However, according to our DQE outcomes, the performance of D-EVO with the CsI screen should not be inferior to other systems based on GOS scintillators.

In Fig. 13 a comparison of the DQE achieved for the two D-EVO systems and some of the best recent data available from the literature is presented, for two different beams (RQA5 and RQA9) at an exposure of 2.5 μGy.[18,19] For RQA5 the D-EVO unit with CsI panel provides DQE outcomes comparable to the best outcomes from other methods based on the same technologies, and similar to others based on an a-Se direct conversion FPD. At higher energies the DQE of the unit based on a-Se detector is worse than the DQE of the CsI systems. This is due to the low atomic number of the Selenium. The DQE of the D-EVO GOS panel is slightly better than that obtained with a unit based on the same technology.

3.C. Contrast-detail analysis

In Table II the IQF outcomes achieved from the CD analysis of the two systems for the four beams at two different dose levels is presented. The mean and the error are computed from averaging the outcomes from the four images acquired for each condition. As expected, the results improve with dose, as demonstrated by the lower IQF values at high exposures. The

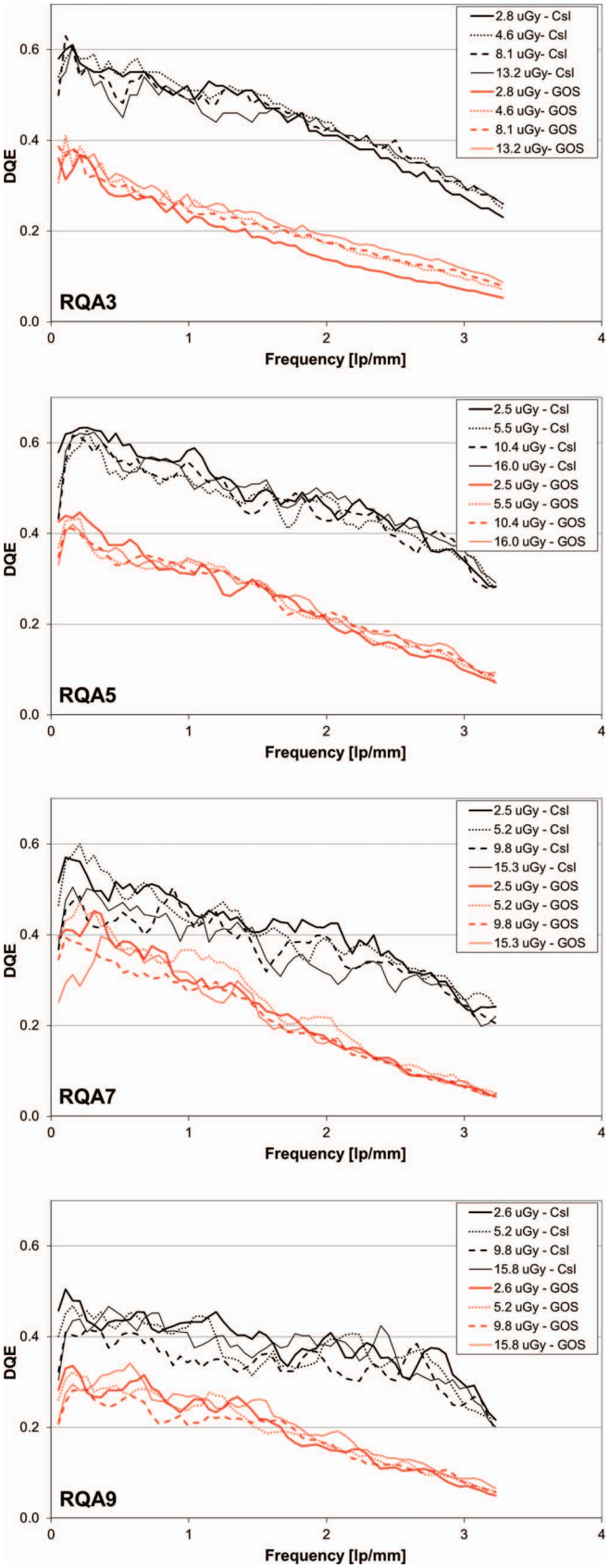

FIG. 11. DQE of the two detectors for the four investigated beams at various exposures. It is worth noting that the DQE of the CsI detector is always better than that obtained with GOS, and both systems present a DQE almost independent from the exposure.

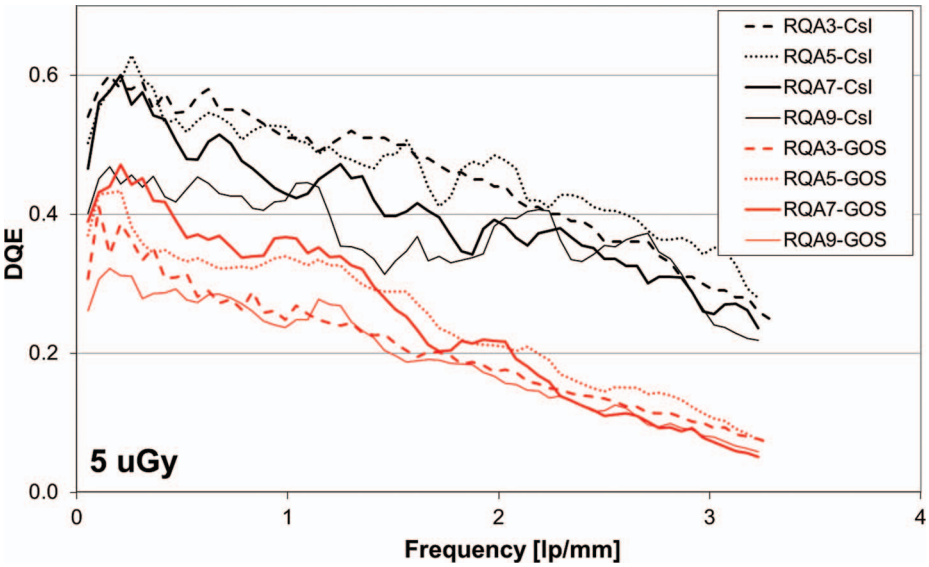

FIG. 12. DQE for the two detectors at an exposure of about 5 μGy for the four considered beams. For both detectors there is a noticeable decrease of DQE for the most energetic beam.

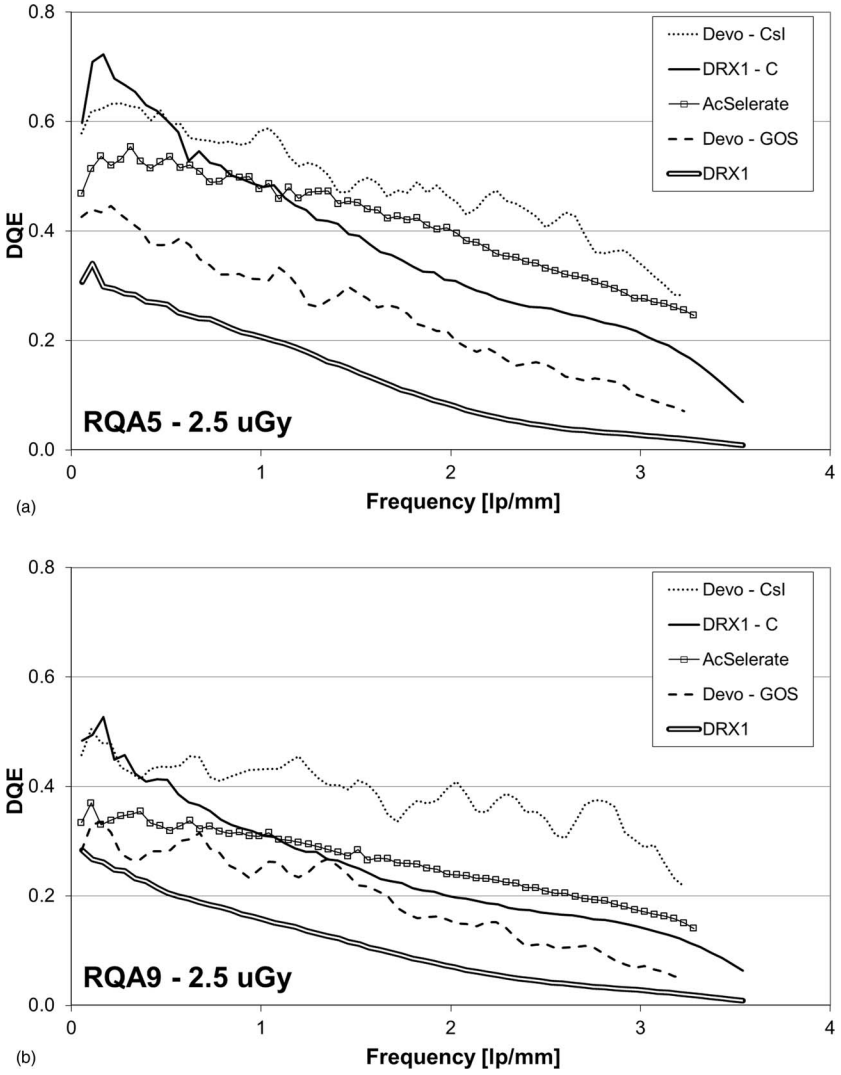

FIG. 13. Comparison of the DQE obtained for the two detectors (D-EVO–CsI and D-EVO–GOS) at an exposure of about 2.5 μGy with some of the best data available from the literature: system based on a thick a-Se layer (AcSelerate), other indirect-conversion systems based on GOS (DRX1) and CsI (DRX1-C) scintillators. (a) RQA5 beam and (b) RQA9 beam.

TABLE II. Values of IQF for all the investigated contrast-detail conditions. Two different dose levels were considered: low (about 2.5 μGy) and high (about 5 μGy).

	GOS		CsI	
X-ray beam	Low dose	High dose	Low dose	High dose
RQA3	0.55 ± 0.05	0.39 ± 0.04	0.47 ± 0.05	0.37 ± 0.03
RQA5	0.43 ± 0.04	0.37 ± 0.03	0.41 ± 0.05	0.34 ± 0.03
RQA7	0.42 ± 0.04	0.34 ± 0.03	0.41 ± 0.04	0.37 ± 0.03
RQA9	0.46 ± 0.05	0.36 ± 0.03	0.47 ± 0.05	0.39 ± 0.04

CD analysis shows that the CsI scintillator performs comparably with the GOS screen in many of the considered conditions. The CsI scintillator is able to provide outcomes better than those obtained with the GOS screen at the lowest energy (RQA3), especially at the lowest dose, where the good noise properties of CsI allow getting a good visibility of the details. In general, a slight improvement of the CsI scintillator can be seen at low energies, whereas for the more energetic beams the performance of the two systems is quite similar. The slightly reduced performance observed for the GOS detector agrees well with data from the literature[6] and also with recent data from mammography systems.[26]

As already observed in previous studies,[33] it is hard to establish a direct relationship between the DQE and the CD response. Though, it seems that the NPS can be a more important feature, for a better comprehension of the CD data. In fact, the differences observed in the DQE for the two phosphors are not reflected in analogous variations in IQF. However, it seems that the NPS outcomes would provide more useful information for understanding the IQF results. Indeed, the noise performance of CsI is remarkably better than that obtained for GOS at low energies, whereas for the two most energetic beams it is comparable or, in some cases, even worse. This is also reflected in the IQF outcomes: the CsI unit is able to provide a more markedly improvement at low energies, whereas at high energies the outcome of the two systems is comparable.

4. CONCLUSION

In this paper we presented a characterization of a new clinical system (named FDR D-EVO) for digital radiography based on an irradiation side sampling technique and equipped with two different scintillators: CsI and GOS.

The limited diffusion of light produced by the ISS reading allows one to achieve a very good spatial resolution. In fact, the MTF of the D-EVO unit is better than most of the systems available on the market, and the CsI panel presents MTF only slightly inferior to that achieved with direct conversion detectors. Thanks to its columnar structure, the CsI scintillator is able to provide an MTF which is remarkably better than that from GOS for all the considered x-ray beams: at the Nyquist frequency (3.33 lp/mm) the MTF is about 35% and 25% for CsI and GOS detectors, respectively.

The CsI scintillator, thanks to the greater thickness of the scintillation layer, can also provide noise properties which are better than the ones from the GOS screen, especially at low energies. The very good MTF, achievable with ISS reading, also affects the NPS shape since the typical steep fall with spatial frequency seen on the scintillator based FPDs can hardly be noticed for the D-EVO system.

The combination of improved spatial resolution, together with the good noise properties reached with the CsI screen, makes possible the achievement of very good DQE outcomes. In fact, the DQE of the CsI system is on average about 1.5 times that of the GOS one, even if the improvement is higher at low energies and lower at high energies. The D-EVO unit with CsI panel is able to provide DQE comparable to the best others based on the same technology and similar to others based on an a-Se direct conversion FPD. The CD analysis shows that the CsI scintillator is able to provide outcomes better than those obtained with the GOS screen at the lowest energy (RQA3), whereas it performs comparably with the GOS screen in many of the other considered conditions.

ACKNOWLEDGMENT

The authors would like to thank Gregorio Benincasa for the assistance in the editing of the manuscript.

[a]Author to whom correspondence should be addressed. Electronic mail: nico.lanconelli@unibo.it; Telephone: +39-051-2095136; URL: www.unibo.it/faculty/nico.lanconelli.

[1]H. P. McAdams, E. Samei, J. Dobbins III, G. D. Tourassi, and C. E. Ravin, "Recent advances in chest radiography," Radiology **241**, 663–683 (2006).
[2]J. Yorkston, "Recent developments in digital radiography detectors," Nucl. Instrum. Methods Phys. Res. A **580**, 974–985 (2007).
[3]C. Schaefer-Prokop, U. Neitzel, H. W. Venema, M. Uffmann, and M. Prokop, "Digital chest radiography: An update on modern technology, dose containment and control of image quality," Eur. Radiol. **18**, 1818–1830 (2008).
[4]N. Tanaka, Y. Yano, H. Yabuuchi, T. Akasaka, M. Sasaki, M. Ohki, and J. Morishita, "Basic imaging properties of an indirect flat-panel detector system employing irradiation side sampling (ISS) technology for chest radiography: Comparison with a computed radiographic system," Radiol. Phys. Technol. **6**(1), 162–169 (2013).
[5]K. Sato, F. Nariyuki, H. Nomura, A. Takasu, S. Fukui, M. Nakatsu, Y. Okada, T. Nabeta, and Y. Hosoi, "Effect of x-ray incident direction and scintillator layer design on image quality of indirect-conversion flat-panel detector with GOS phosphor," Proc. SPIE **7961**, 79614I-1–79614I-8 (2011).
[6]N. W. Marshall, A. Mackenzie, and I. D. Honey, "Quality control measurements for digital x-ray detectors," Phys. Med. Biol. **56**, 979–999 (2011).
[7]International Electrotechnical Commission, "Medical diagnostic x-ray equipment—Radiation conditions for use in the determination of characteristics," *IEC-61267, Geneva, Switzerland*, 2003.
[8]W. Zhao and J. A. Rowlands, "X-ray imaging using amorphous selenium: Feasibility of a flat panel self-scanned detector for digital radiology," Med. Phys. **22**(10), 1595–1604 (1995).
[9]E. Samei and M. J. Flynn, "An experimental comparison of detector performance for computed radiography systems," Med. Phys. **29**(4), 447–459 (2002).
[10]G. Borasi, A. Nitrosi, P. Ferrari, and D. Tassoni, "On site evaluation of three flat panel detectors for digital radiography," Med. Phys. **30**, 1719–1731 (2003).
[11]E. Samei and M. J. Flynn, "An experimental comparison of detector performance for direct and indirect digital radiography systems," Med. Phys. **30**(4), 608–622 (2003).

[12]U. Neitzel, S. Gunther-Kohfahl, G. Borasi, and E. Samei, "Determination of the detective quantum efficiency of a digital x-ray detector: Comparison of three evaluations using a common image data set," Med. Phys. **31**(8), 2205–2211 (2004).
[13]G. Borasi, E. Samei, M. Bertolini, A. Nitrosi, and D. Tassoni, "Contrast-detail analysis of three flat panel detectors for digital radiography," Med. Phys. **33**(6), 1707–1719 (2006).
[14]J. T. Dobbins III, E. Samei, N. T. Ranger, and Y. Chen, "Intercomparison of methods for image quality characterization. II. Noise power spectrum," Med. Phys. **33**(5), 1466–1475 (2006).
[15]P. Monnin, Z. Hotzer, R. Wolf, U. Neitzel, P. Vock, F. Gudinchet, and F. R. Verdun, "An image quality comparison of standard and dual-side read CR systems for pediatric radiology," Med. Phys. **33**(2), 411–420 (2006).
[16]L. Riccardi, M. C. Cauzzo, R. Fabbris, E. Tonini, and R. Righetto, "Comparison between a built-in dual side chest imaging device and a standard single side CR," Med. Phys. **34**(1), 119–126 (2007).
[17]S. Rivetti, N. Lanconelli, M. Bertolini, A. Nitrosi, A. Burani, and D. Acchiappati, "Comparison of different computed radiography systems: Physical characterization and contrast detail analysis," Med. Phys. **37**, 440–448 (2010).
[18]S. Rivetti, N. Lanconelli, M. Bertolini, and D. Acchiappati, "A new clinical unit for digital radiography based on a thick amorphous Selenium plate: Physical and psychophysical characterization," Med. Phys. **38**, 4480–4488 (2011).
[19]M. Bertolini, A. Nitrosi, S. Rivetti, N. Lanconelli, P. Pattacini, V. Ginocchi, and M. Iori, "A comparison of digital radiography systems in terms of effective detective quantum efficiency," Med. Phys. **39**, 2617–2627 (2012).
[20]C. E. Floyd Jr., R. J. Warp, J. T. Dobbins III, H. G. Chotas, A. H. Baydush, R. Vargas-Voracek, and C. E. Ravin, "Imaging characteristics of an amorphous silicon flat-panel detector for digital chest radiography," Radiology **218**, 683–688 (2001).
[21]K. A. Fetterly and B. A. Schueler, "Performance evaluation of a dual-side read dedicated mammography computed radiography system," Med. Phys. **30**(7), 1843–1854 (2003).
[22]K. A. Fetterly and B. A. Schueler, "Performance evaluation of a computed radiography imaging device using a typical front side and novel dual side readout storage phosphors," Med. Phys. **33**(2), 290–296 (2006).
[23]International Electrotechnical Commission, "Medical electrical equipment—Characteristics of digital X-ray imaging devices—Part 1: Determination of the detective quantum efficiency," *IEC-62220-1, Geneva, Switzerland*, 2003.
[24]G. Poludniowski, G. Landry, F. DeBlois, P. M. Evans, and F. Verhaegen, "SpekCalc: A program to calculate photon spectra from tungsten anode x-ray tubes," Phys. Med. Biol. **54**, N433–N438 (2009).
[25]P. Monnin, D. Gutierrez, S. Bulling, D. Lepori, J. F. Valley, and F. R. Verdun, "Performance comparison of an active matrix flat panel imager, computed radiography system, and a screen-film system at four standard radiation qualities," Med. Phys. **32**, 343–350 (2005).
[26]N. W. Marshall, K. Lemmens, and H. Bosmans, "Physical evaluation of a needle photostimulable phosphor based CR mammography system," Med. Phys. **39**, 811–824 (2012).
[27]N. W. Marshall, P. Monnin, H. Bosmans, F. O. Bochud, and F. R. Verdun, "Image quality assessment in digital mammography: Part I. Technical characterization of the systems," Phys. Med. Biol. **56**, 4201–4220 (2011).
[28]S. Rivetti, N. Lanconelli, M. Bertolini, G. Borasi, P. Golinelli, D. Acchiappati, and E. Gallo, "Physical and psychophysical characterization of a novel clinical system for digital mammography," Med. Phys. **36**, 5139–5148 (2009).
[29]E. Samei, "Image quality in two phosphor-based flat panel digital radiographic detectors," Med. Phys. **30**(7), 1747–1757 (2003).
[30]A. Mackenzie and I. D. Honey, "Characterization of noise sources for two generations of computed radiography systems using powder and crystalline photostimulable phosphors," Med. Phys. **34**(8), 3345–3357 (2007).
[31]M. Matsumoto, T. Yamazaki, M. Nokita, S. Hayashida, A. Yoshida, T. Ideguchi, K. Himuro, M. Ohki, S. Kumazawa, and Y. Higashida, "Physical imaging properties and low-contrast performance of a newly developed flat-panel digital radiographic system," Jpn. J. Radiol. Technol. **61**(12), 1656–1665 (2005).
[32]E. Samei, N. T. Ranger, J. T. Dobbins III, and C. E. Ravin, "Effective dose efficiency: An application-specific metric of quality and dose for digital radiography," Phys. Med. Biol. **56**, 5099–5118 (2011).
[33]S. Rivetti, N. Lanconelli, R. Campanini, M. Bertolini, G. Borasi, A. Nitrosi, C. Danielli, L. Angelini, and S. Maggi, "Comparison of different commercial FFDM units by means of physical characterization and contrast-detail analysis," Med. Phys. **33**(11), 4198–4209 (2006).